

Characterization and Traversal of Pliable Vegetation for Robot Navigation

Camilo Ordonez¹, Ryan Alicea¹, Brandon Rothrock², Kyle Ladyko¹, Jeremy Nash², Rohan Thakker², Shreyansh Daftry², Mario Harper¹, Emmanuel Collins¹, and Larry Matthies²

¹ Florida State University, Tallahassee, FL 32310

² Jet Propulsion Laboratory, Pasadena, USA

Abstract. Outdoor mobile robots currently treat vegetation as obstacles that need to be avoided. In order to have less conservative robots that fully exploit their motion capabilities, it is required to obtain models of the interaction of vegetation with the vehicle. This work proposes and experimentally verifies models of interaction of wheeled and tracked vehicles with pliable vegetation. In addition, a methodology to map perceptual features of the environment to resistive forces experienced by the robots is presented.

1 Introduction

Vegetated terrains are pervasive in the real world and thus it is crucial for autonomous systems to be able to treat them in a non-binary fashion. That is, robots should be able to reason about the vegetation in their surroundings and decide if and how to traverse such challenges. Of particular interest are terrains that are taller than or of comparable height to the vehicle hull (hereafter referred to as tall vegetation).

Current state of the art utilizes a conservative approach that classifies such vegetated terrains as obstacles and then plans routes that navigate around them. For example, dense point clouds obtained using lidar data have been used to segregate the environment into classes representing whether the terrain was traversable or non-traversable [1]. Also, the spaces between foliage have been used as the workspace within which paths could be generated [2].

In relevant work on identification of vegetated terrain, a multispectral sensor was created out of a near-infrared camera and a visible light video camera [3], leading to a robust chlorophyll detector in natural environments. Additional work focused on segmentation of lidar data into three classes using local three-dimensional point cloud statistics [4], [5]. A perception methodology more geared towards vegetation traversal has also been developed [6]. In that research a combination of lidar and radar was employed to detect large tree trunks that can be occluded behind thick foliage.

A 3D algorithm to detect and classify obstacles has also been proposed [7]. The approach classifies the obstacles as belonging to different obstacle types

(rocks, vegetation, etc). It also included a terrain load bearing model, which was coupled with a suspension model of the vehicle to generate estimates of safe traversal speeds for the different terrains. Vegetation traversal has been studied [8], where uniform patches of vegetation were characterized using a lumped frictional model. The developed terrain models were then used to plan trajectories that exploited the vehicle momentum to traverse the vegetation patches while avoiding vehicle immobilization. More detailed stem models of vegetation have been proposed [9]. However, that work was limited to simulations and did not incorporate perception.

In this paper, we propose two different yet complementary approaches to characterize pliable terrains. One approach relies on traversals of the terrain and measurements of proprioceptive data to estimate a lumped resistance force experienced by the vehicle. The second approach relies on probing the terrain via a manipulator equipped with a torque-force sensor. Using this data, a physics-based model of the local vegetation is developed. In addition, this work presents a regression model which learns the mapping between perceptual features from exteroceptive sensors to interaction forces between the robot and the vegetation. The remainder of the paper is structured as follows: Section 2 describes the experimental platforms, Section 3 details the technical approach, Section 4 summarizes the experimental results, and Section 5 contains concluding remarks and future work.

2 Experimental Platforms

As shown in Fig. 1, this work utilizes two robotic platforms. The Roman tracked vehicle equipped with a Robosimian 7 degree of freedom manipulator developed at JPL, a Velodyne VPL-16 lidar, and 3 Intel RealSense ZR300 cameras. The second robot is a Husky skid steered vehicle from ClearPath equipped with a Velodyne VPL-16 lidar, 2 Intel RealSense ZR300's, current sensors per motor, a Microstrain 3DM-GX3-25 IMU, and a force bumper developed in-house containing two front-facing load cells.

3 Technical Approach

The overall approach is decomposed into two stages. A terrain modeling and characterization module and a regression system to map from perception data into resistance forces experienced by the robot.

3.1 Vegetation Characterization

Due to the different capabilities of the robots employed, the terrain modeling is platform dependent and is conducted as detailed below.

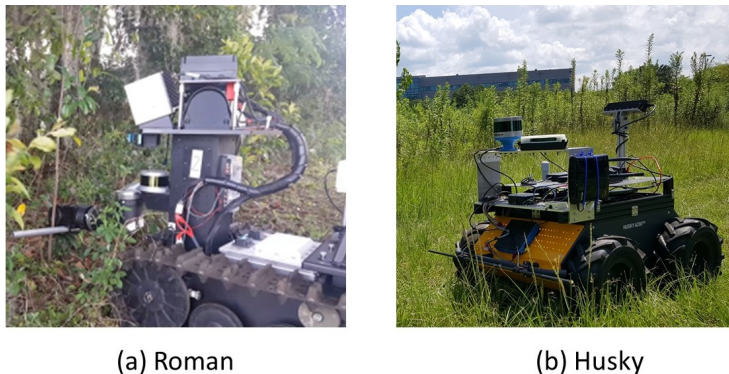


Fig. 1. Experimental platforms used in this work. (a) The tracked Roman platform equipped with a manipulator to probe the terrain. (b) The skid steered Husky robot.

Terrain Modeling with the Roman: Given the manipulator available on the Roman, it is possible to conduct a bottom up approach to terrain characterization. As illustrated in Fig. 2, the approach starts by modeling stems of vegetation as thin rods anchored on the ground, with rotational stiffness k , and rotational damping b . The second order linear differential equation describing the unforced dynamics of the stem can be expressed by

$$J\ddot{\theta} + b\dot{\theta} + k\theta = 0, \quad (1)$$

where J is the stem's moment of inertia, θ is the angle of the stem, and $\dot{\theta}$ and $\ddot{\theta}$ are its angular velocity and acceleration.

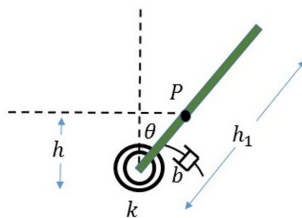


Fig. 2. Model of a vegetation stem of length h_1 , rotational stiffness k and rotational damping b . Here, h represents the location at which an external force F interacts with the stem.

The robot longitudinal dynamics when interacting with one or more stems can be expressed as

$$M\ddot{x} + D(x, \dot{x}) + R_{res} = F, \quad (2)$$

where M is the robot's mass and F is the tractive force exerted by the robot tracks on the terrain. This force is required to accelerate the vehicle and to

overcome the rolling resistance R_{res} and the drag D generated by the tall vegetation. Here, we assume that the terrain underneath the vegetation has the same properties as non-vegetated terrain in its proximity.

Assuming a very small stem inertia J , and given that the robot bumper makes contact with the stems at a height h , one can model the drag on the robot resulting from n stems using

$$D = \frac{1}{h} \sum_{i=1}^n \alpha_i k_i \theta_i \cos^2 \theta_i + \frac{1}{h} \sum_{i=1}^n \alpha_i b_i \dot{\theta}_i \cos^2 \theta_i, \quad (3)$$

where $\alpha_i = 1$ if stem i is in contact with the vehicle, and 0 otherwise.

Terrain Modeling with the Husky: in the absence of a manipulator, it is complicated to capture the interaction of individual stems. In addition, although it is expected that the overall resistance force varies with robot velocity, it was found that in practice is very complicated to traverse the same region twice at different speeds because during the first traversal the robot permanently destroys some of the vegetation. For these reasons, in the case of the Husky robot, the resistance of the vegetation is modeled via a lumped force f . Assuming an applied tractive force F , vehicle mass M , and acceleration a , the robot forward dynamics are governed by

$$F - f = Ma. \quad (4)$$

As the robot moves through the terrain, F is estimated from the current sensors using $F = \frac{\eta k_t G_r}{R} (i_l + i_r)$, where k_t is the torque constant, G_r is the gear ratio of the motor, R is the wheel radius, i_l and i_r are the left and right motor currents, and η is the efficiency of the motor and gearbox.

Employing a grid based map of the terrain as shown in Fig. 3, the net resistance f^k experienced by the vehicle at time k is given by

$$f^k = \sum_{i=1}^n \frac{\alpha_i^k f_i}{l}, \quad (5)$$

where n is the number of cells in the map, α_i^k is the overlap-length of the vehicle with cell i at time k , f_i is the resistance force of cell i and l is the length of the robot.

In the field, the resistance values f_i for each cell are estimated as follows: the robot is commanded to move in straight line at constant velocity. Then, provided the robot localization, the instantaneous robot-cell overlap values α_i^k are computed. To account for small accelerations imposed by the controller and ground interaction, the robot acceleration a^k is measured with an on board IMU. Combining (4) and (5),

$$F^k - Ma^k = \sum_{i=1}^n \frac{\alpha_i^k f_i}{l} \quad (6)$$

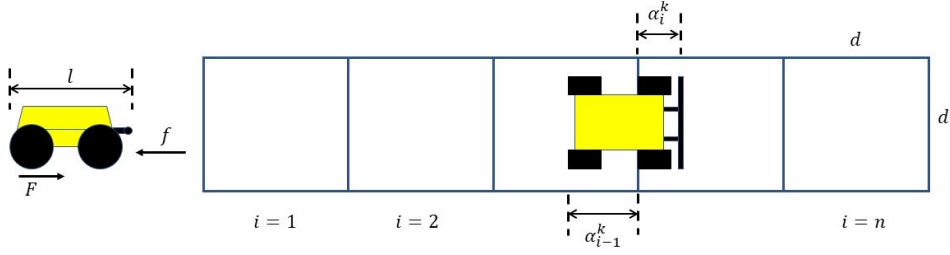


Fig. 3. Vehicle terrain interaction model for the Husky. A lumped resistance force f_i is estimated for each grid cell in the robot map. Each cell is assumed of size $d \times d$. α_i^k represents the overlap length of the vehicle with cell i at time k .

As the robot moves through the terrain, it is possible to obtain m observations of (6) and estimate the unknown cell resistance forces using linear least squares as follows:

$$Y = Hq + \epsilon, \quad (7)$$

where

$$Y = \begin{bmatrix} F^1 - Ma^1 \\ F^2 - Ma^2 \\ \vdots \\ F^m - Ma^m \end{bmatrix}, \quad H = \begin{bmatrix} \frac{\alpha_1^1}{l} & \frac{\alpha_2^1}{l} & \dots & \frac{\alpha_n^1}{l} \\ \frac{\alpha_1^2}{l} & \frac{\alpha_2^2}{l} & \dots & \frac{\alpha_n^2}{l} \\ \vdots & \vdots & \ddots & \vdots \\ \frac{\alpha_1^m}{l} & \frac{\alpha_2^m}{l} & \dots & \frac{\alpha_n^m}{l} \end{bmatrix}, \quad \text{and } q = \begin{bmatrix} f_1 \\ f_2 \\ \vdots \\ f_n \end{bmatrix},$$

ϵ represents the error in the resistance force prediction. Since (7) is an overdetermined system, q is estimated as the least squares solution, $\hat{q} = (H^T H)^{-1} H^T Y$.

3.2 Mapping from Perception to Resistance Force

The objectives of the perception system is to predict terrain properties from vision and lidar sensors. The current and force measurements are used to directly estimate the lumped resistance directly underneath the robot as described above. These estimated parameters are accumulated into a 3D voxel grid, and used to train a prediction model to infer these parameters on a local region of the map surrounding the robot. The voxel resolution we are using is 5cm^3 .

The vision sensors used on the robot consist of Intel RealSense ZR300 assisted stereo cameras and a VLP-16 lidar. The stereo cameras are primarily used for localization using ORB-SLAM2 [11]. The 3D voxel map is based on the JMS architecture described in [12], and is populated using lidar data. We use the multi-return mode of the Velodyne to record both the strongest and last return, illustrated in Figure 5, to predict vegetation density. The mean difference between these two returns is stored for each voxel. The resulting voxel map contains a single scaler for each cell, and is processed in $5 \times 5 \times 5$ voxel subvolumes by the prediction model.

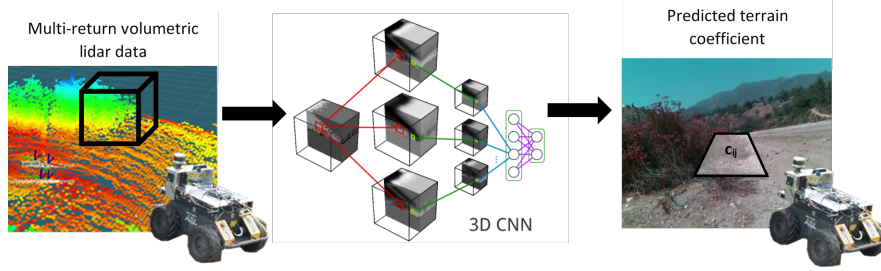


Fig. 4. Overview of the terrain prediction system. The terrain is divided into 25cm^3 subvolumes indicated by the box outline. Multi-return statistics are collected from the lidar to populate each 5cm^3 voxel in the map, which is then processed by a 3D CNN to predict resistance values for each subvolume. See text for details.

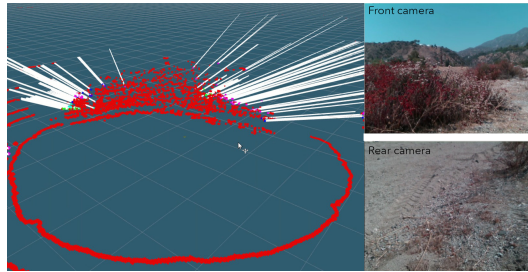


Fig. 5. Velodyne multi-return mode consists of the strongest (red dot) and last return (white ray), which measures how well the laser can penetrate through the vegetation, and helps predict vegetation density.

The prediction model is based on a volumetric convolutional neural network [13]. The CNN model utilizes 3D convolution to reason about local spatial context, followed by a dense fully-connected layer and a regression output layer, as shown in Figure 4. The loss function is a regularized negative log-likelihood, optimized using stochastic gradient descent. The input to the network is a 3D tensor containing a subvolume of the map with dimensions $25\text{m} \times 25\text{m} \times 25\text{m}$. The output is the lumped resistance, as described above, and is run as a sliding window within the region of interest.

4 Results

This section presents results of vegetation characterization with the both platforms and perception results on the Husky.

4.1 Roman Platform

The unforced dynamics of the stem were experimentally verified on real vegetation with high speed video in previous work [9]. Here, field experiments were

conducted on scenarios like the one of Fig. 6b. A rigid bar with a width equivalent to that of the robot was held by the gripper to capture the full resistance which would be experienced by the robot during traversal. The end-effector position trajectory of Fig. 6a was commanded. During each probe, the manipulator pushed the bar forward in order to deflect an area of vegetation. While the vegetation was held at a constant deflection, the forces seen by the force plate at the wrist were used to estimate the stiffness, k , of the vegetation. Once the stiffness was estimated, the damping component, b , was obtained by analysis of the constant velocity periods of the probe.

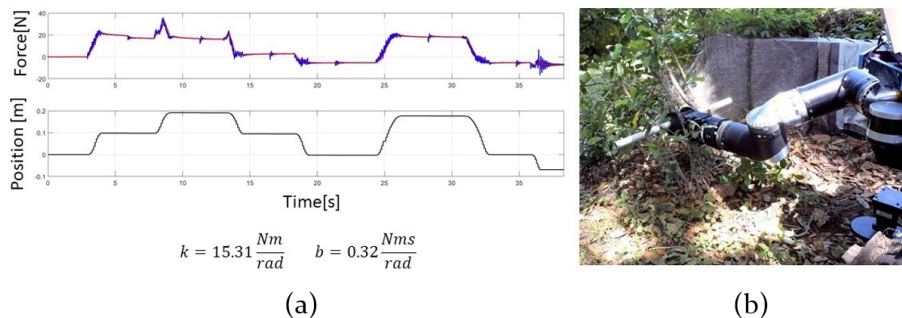


Fig. 6. Estimation of stem model parameters (k, b) through manipulation. The manipulator pushes the stem by following the shown displacement trajectory. The force plot corresponds to the normal force sensed by the torque-force sensor installed in the wrist of the arm. The regions of the trajectory where the arm maintains a constant position are used to estimate k and regions of constant velocity are used to estimate b .

The estimated stem models can then be used to quantify the difficulty of traversal through a patch of vegetation. A traversal experiment was conducted in the scenario shown in Fig. 7a. First, the manipulator was used to obtain a lumped stiffness and damping value for each grouping of stems. This was done by probing each patch from different orientation angles. The rolling resistance on the terrain was estimated by driving the vehicle at constant speed, 0.55m/s, on flat ground adjacent to the vegetation clusters under observation. From forward simulations of the vehicle dynamics using (2), the energetic cost of traversal was computed as $E = \int_0^t Fv dt$, where F is the applied tractive force and v is the robot velocity. Energetic costs only include the period of time which the robot was in contact with the stem.

The energetic cost required to traverse the area in Fig. 7a was measured to be 767J while the predicted value was 620J, resulting in a percent error of 19.14%.

In Fig. 8, a more practical situation is presented in which the robot is required to traverse a patch of randomly distributed stems with known stiffness and damping properties. A Particle Swarm Optimization method [10] was implemented in order to find the optimal entry point (vehicle position along the Y-axis



Fig. 7. The vegetated areas used to validate the stem model with the Roman. (a) Leafy and dense underbrush ($k: 96.34 \frac{Nm}{rad}$; $b: 70.9 \frac{Nms}{rad}$) (b) Cluster of thin saplings ($k: 159.0 \frac{Nm}{rad}$; $b: 80.2 \frac{Nms}{rad}$).

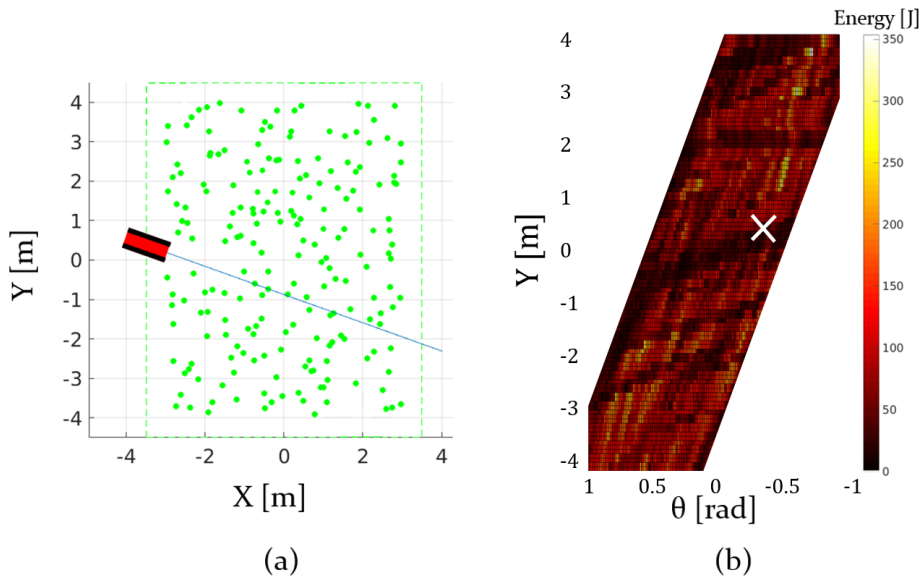


Fig. 8. (a) Vegetation patch with randomly distributed stems. (b) Energetic cost of traversal of the vegetation patch from different entry positions and orientations. The lowest cost entry configuration is highlighted with an X . Rolling resistance was ignored in these simulations.

and orientation with respect to the X-axis) to the patch to yield the minimum energetic cost of traversal. In the optimization, the vehicle was constrained to

move in rectilinear motion but with an arbitrary heading such that the vehicle traversed the full width of the patch.

4.2 Husky Platform

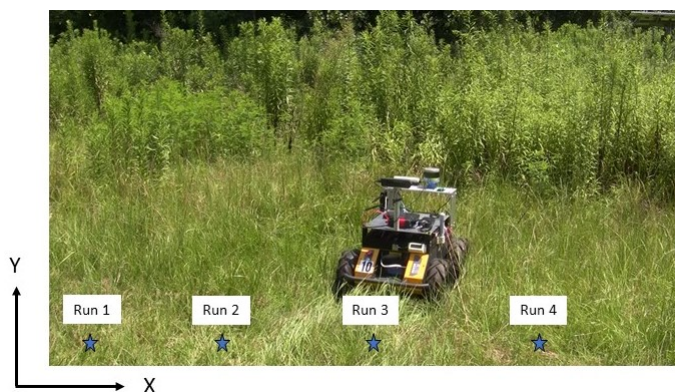


Fig. 9. Husky traversing a vegetation patch from different starting positions.

Estimation of lumped resistance force: The Husky robot was commanded to traverse the vegetated terrain shown in Fig. 9 from four different starting locations. In all experiments, the robot moved in a straight line and low level data including currents, position, and IMU was logged. One run was performed at a speed of $0.25m/s$ and was employed to estimate the resistance force from each cell via the method described in Section 3.1. The estimation results are summarized in Fig. 10. Runs 2 and 3 were performed at $0.5m/s$ and run 4 at $1m/s$. In all these runs, the vehicle started on short grass, transitioned to medium grass, and finished on dense brush, which correlates with the estimated resistance values of Fig. 10.



Fig. 10. Estimated lumped resistance force per cell. Each cell has a size of $1m \times 1m$

Once the lumped resistance forces per cell are estimated, a forward simulation of the vehicle over the terrain can be performed and used to compare the predicted vs actual energy mechanical energy required to traverse the vegetation patch. Fig. 11 shows a typical energy comparison in the scenario of Fig. 9. The

errors in energy predictions for the four experimental runs are summarized in Table 1.

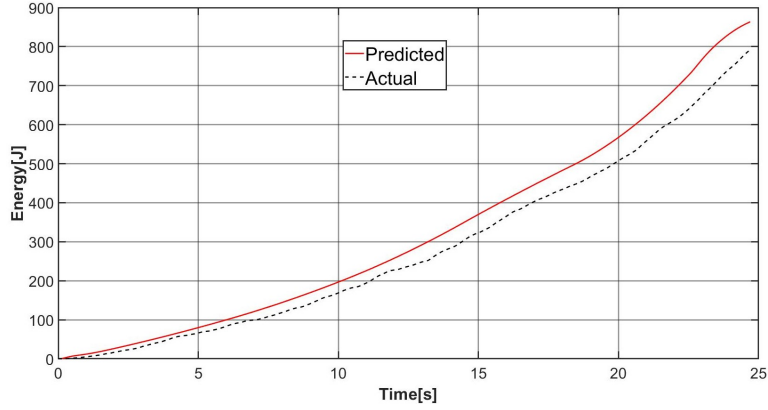


Fig. 11. Predicted vs. experimental mechanical energy.

Table 1. Energy prediction errors

Run	Speed[m/s]	Energy prediction error[%]
1	0.25	9.01
2	0.50	11.97
3	0.50	14.22
4	1.00	23.25

Perception: Our experiments are conducted on a region of terrain approximately $100m$ in length that is traversed with the Husky robot. This environment contains a diversity of vegetation that includes dirt, light traversable vegetation, and heavy brush that is mostly untraversable. Lumped resistance is recorded along the traverse path of the robot, and is used to train the prediction model in a self-supervised manner. For these experiments, some of the terrain is dense enough to completely halt the robot and violate the constant velocity assumption. These discrepancies were manually removed and reannotated to provide a cleaner map for training the prediction algorithm.

Figure 12 illustrates some example results from our prediction model. The left image contains an elevation map to illustrate the locations of the vegetation. The black line through the center of the map illustrates the traverse path of the robot. The right image shows the output of the terrain predictions overlaid on the map, with red being the highest resistance, and green the lowest. Note that the bands on the bottom of the image are artifacts from humans walking along side the robot, which are correctly filtered out by the model. For evaluation,

we discretize the lumped resistance into three classes of zero, light, and heavy resistance, and measure accuracy simply as classification error. Using a 4-fold cross-validation, our model has a prediction accuracy of 74% in this scenario.

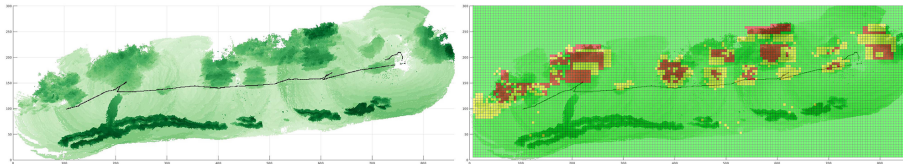


Fig. 12. Terrain classification results. The left image shows an elevation map of the terrain, with the traverse path of the robot illustrated by the black line. The right image shows the predicted lumped resistance overlaid over the map.

5 Conclusions and Future Work

This work developed two different methodologies to characterize the interaction of a vehicle with pliable vegetation. One approach is suitable for robots equipped with a manipulator and characterizes the local terrain by using a stem model with experimentally estimated rotational stiffness and damping properties. The second approach relies on motor current sensing to characterize the local terrain via a lumped resistance force. Both approaches were experimentally validated on short vegetation patches $\approx 6m$ and were shown to provide energy prediction errors of less than 20%.

Additionally, an approach based on particle swarm optimization was developed in simulation to determine the optimal entry pose to a vegetation patch of randomly distributed stems.

The approach to perception shows promise in its ability to predict the resistance to traversal in previously unexplored regions. Though as the length of the trajectory increases and the terrain becomes more varied, the quality with which the existing sensors and terrain model are able capture the terrain interaction begins to degrade. This produces a noisy ground-truth signal for the perception system leading to a reduction in prediction performance. Future designs can likely be improved by better sensor design and placement as well as higher fidelity terrain models.

Several important challenges remain open such as autonomous selection of probing regions on the vegetation, dealing with occlusions, and estimation of overall patch geometry prior to traversal. It is expected that some of these challenges can be alleviated via cooperation with an aerial vehicle. Future work will explore the coupling of the proposed methodology with a sampling based motion planner to autonomously generate energy-efficient trajectories. In addition, this work will be applied to legged platforms.

6 Acknowledgements

This work was supported by the collaborative participation in the Robotics Consortium sponsored by the U.S. Army Research Laboratory under the Collaborative Technology Alliance Program, Cooperative Agreement DAAD 19-01-2-0012. The U.S. Government is authorized to reproduce and distribute reprints for Government purposes not withstanding any copyright notation thereon.

References

1. Krusi, P., Furgake, P., Bosse, M., Siegwart, R.: Driving on point clouds: Motion planning, trajectory optimization, and terrain assessment in generic nonplanar environments. *Journal of Field Robotics* 34(5), 940-984 (2017)
2. Vandapel, N., Kuffner, J., Amidi, O.: Planning 3-d path networks in unstructured environments. In: *IEEE International Conference on Robotics and Automation*, pp. 4624-4629. Barcelona (2005)
3. Bradley, D., Thayer, S., Stentz, A., and Rander, P.: Vegetation detection for mobile robot navigation. Technical Report, (2003)
4. Hebert, M. and Vandapel, N.: terrain classification techniques from ladar data for autonomous navigation. In: *Collaborative Technology Alliances conference*, (2003)
5. Lalonde, J., Vandapel, N., Huber, D., Hebert, M.: Natural terrain classification using threedimensional ladar data for ground robot mobility. *Journal of Field Robotics* 23, 839-861 (2006)
6. Matthies, L., Bergh, C., Castano, A., MAcedo, J., Manduchi, R.,: Obstacle detection in foliage with ladar and radar. In: *International Symposium of Robotics Research*, (2003)
7. Talukder, A., Manduchi, R., Owens, K., Matthies, L., Castano, A., and Hogg, R.: Autonomous terrain characterization and modeling for dynamic control of unmanned vehicles. In: *IEEE/RSJ Conference on Intelligent Robots and Systems (IROS)*, (2002)
8. Ordonez, C., Gupta, N., Chuy, O., and Collins, E.: Momentum based traversal of mobility challenges for autonomous ground vehicles. In: *IEEE International Conference on Robotics and Automation*, (2013)
9. Ordonez, C., Alicea, R., Rothrock, B., Ladyko, K., Harper, M. Karumanchi, S., Matthies, L., Collins, E.: Modeling and Traversal of Pliable Materials for Tracked Robot Navigation. In: *SPIE Defense, Security, and Sensing Conference Unmanned Systems Technology XIX*, (2018)
10. Trelea. I.C: The particle swarm optimization algorithm: convergence analysis and parameter selection. In: *Information processing letters*, Vol. 85, No. 6 (2003)
11. Mur-Artal R, Tards JD. Orb-slam2: An open-source slam system for monocular, stereo, and rgb-d cameras. *IEEE Transactions on Robotics*. (2017)
12. Bajracharya M, Ma J, Howard A, Matthies L. Real-time 3d stereo mapping in complex dynamic environments. In *International Conference on Robotics and Automation-Semantic Mapping, Perception, and Exploration (SPME) Workshop* (2012)
13. Maturana D, Scherer S. Voxnet: A 3d convolutional neural network for real-time object recognition. *Intelligent Robots and Systems (IROS)*, 2015 *IEEE/RSJ International Conference* (2015)